Journal of the European Ceramic Society 20 (2000) 2367–2376

Perovskite forming ceramics of the system $Sr_xLa_{1-x}\ Ti^{IV}_{x+y}Co^{II}_{y}Co^{III}_{1-x-2y}O_3$ for NTC thermistor applications

Adalbert Feltz *

Electronic Parts and Components, Keramische Bauelemente EPCOS KB, Siemensstraâe 43, A-8530 Deutschlandsberg, Austria

Received 14 February 2000; received in revised form 17 April 2000; accepted 29 April 2000

Abstract

The paper reports the preparation, structure and electrical properties of oxide ceramic semiconductors based on the series $Sr_xLa_{1-x}Ti^{IV}_{x+y}Co^{II}_{y}Co^{III}_{1-x-2y}O_3$ with perovskite type stucture: $0<x<1$, $0<y<(1-x)/2$. The study starts from $LaCoO_3$ which is highly conductive yielding metallic condutivity above 330°C. The upset trigonal distortion of $LaCoO_3$ is reduced when Sr^{II}/Ti^{IV} is substituted for La^{III}/Co^{III} corresponding to increasing values of x and also when 2 Co^{III} are introduced for Ti^{IV}/Co^{II} into the lattice corresponding to increasing values of y. At high values of x and y othorhombic distortion occurs. At the same time, the interaction between the Co^{III} atoms of $LaCoO_3$ is increasingly interrupted providing increasing values of the the resistivity value $\rho_{25°C}$ and of the $B_{25/100°C}$ value deduced from measurements at 25 and 100°C according to $\rho(T)=\rho_{25°C}\ e^{B/T}$. The range of variation of x an y makes possible to prepare ceramics with desired electrical properties within the limits of $\rho_{25°C}=1.1$ Ωcm, $B=1910$ K and $\rho_{25°C}=1$ bis 8×10^6 Ωcm at B-values up to 6500 K. Dependent on composition, NTC ceramics for thermistor or insurance applications are accessible. Thermistors do not show aging even at higher temperature, e.g. at 500°C, provided the single phase state is achieved as a result of mixed oxide preparation and sintering. Hence, high temperature thermistor applications are also made possible. The semiconductor behavior can be understood using the conventional polaron state hopping model.

Keywords: Electrical properties; NTC; Perovskite; $(Sr,La)(Ti,Co)O_3$; Thermistors

Zusammenfassung

Es wird über Darstellung, Struktur und elektrische Eigenschaften oxidkeramischer Halbleiter auf der Basis von Perowskiten der allgemeinen Zusammensetzung $Sr_xLa_{1-x}Ti^{IV}_{x+y}Co^{II}_{y}Co^{III}_{1-x-2y}O_3$ mit $0<x<1$ und $0<y<(1-x)/2$ berichtet. Die trigonale Stauchung der Perowskitstruktur von $LaCoO_3$ erfährt mit zunehmender Substitution von La^{III}/Co^{III} durch Sr^{II}/Ti^{IV} entsprechend einer Zunahme von x und von 2 Co^{III} durch Ti^{IV}/Co^{II} entsprechend einer Zunahme von y eine Abschwächung. Sie geht bei hohen x- und y- Werten in eine orthorhombische Verzerrung über. Zugleich wird die Wechselwirkung zwischen den Co^{III} - Atomen im $LaCoO_3$, die ab 330°C zu metallischer Leitfähigkeit führt, zunehmend unterbrochen, was einen Widerstandsanstieg und einen höheren B - Wert hervorruft. Im Variationsbereich von x und y sind spezifische Widerstände $\rho_{25°C}$ und $B_{25/100°C}$- Werte, letztere aus Messungen bei 25 und 100°C gemäß $\rho(T)=\rho_{25°C}\ e^{B/T}$, zwischen $\rho_{25°C}=1{,}1$ Ωcm, B = 1910 K und $\rho_{25°C}=1$ bis 8×10^6 Ωcm bei B - Werten bis zu 6500 K zugänglich. Je nach Zusammensetzung lassen sich aus derartigen NTC- Keramiken Einschaltheißleiter oder Temperaturfühler (Thermistoren) herstellen. Unter der Voraussetzung, daß bei der Masseaufbereitung nach dem Mixed Oxide Verfahren und durch Sintern die Ausbildung der einphasigen Perowskitphase zustande kommt, weisen derartige Keramikbauelemente in nicht reduzierender Atmosphäre, z. B. an Luft, auch im Bereich höherer Temperatur, z. B. 500°C, praktisch keine Alterung auf. Das Leitfähigkeitsverhalten kann im Rahmen des aus der Literatur bekannten Polaronen- Transportmodels beschrieben werden.

* Tel.: +43-3462-800-2410; fax: +43-3462-800-373.
E-mail address: adalbertfeltz@siemens.dlbl.de or adalbert.feltz@epcos.com

0955-2219/00/$ - see front matter
PII: S0955-2219(00)00149-7

1. Introduction

By reason of increasing changes of the electrical data with time, the application of NTC thermistors based on spinel forming transition metal oxide systems is commonly limited to temperatures below about 200°C. Previous studies[1] on ceramics of the system $Fe_x^{III}Ni_y^{II}Mn_{3-x-y}^{z}O_{3+x/2+\delta}$ with $z=[2\delta/(3-x-y)]+2$ revealed that the changes of the electrical properties with time arise predominantly from losing the frozen-in state of the equilibrium of distribution of cations between the tetrahedral and octahedral sites of the spinel structure and less from phase heterogeneity which often is a result of partial decomposition or incomplete formation of the spinel phase at sintering. On the other hand, the single phase spinel compound $FeNi_{0.5}Mn_{1.5}O_4$ was found to be stable up to about 1415°C which makes possible sintering without decomposition. Cation redistribution occurs without phase transition. However, only above about 400°C the relaxation of equilibrium adjustment of cation redistribution can follow the conventional rates of temperature changing. Hence, above this range of temperature, $FeNi_{0.5}Mn_{1.5}O_4$ ceramics fulfil all of the requirements of a material for high temperature NTC thermistor applications.[2] Corresponding to $\alpha=-B/T^2$ the B constant of 7470 K provides a sensitivity $\alpha=0.5\%$ in the range of 1000°C without aging.

The compound $Sr_7Mn_4O_{15}$, whose constitution is a double octahedra version of the K_2NiF_4 type structure,[3] has also been proposed for high temperature NTC thermistor applications.[4,5] Due to the high value of the B constant of 14350 K, a sensitivity of 0.9% is found even at 1000°C.[6] On the other hand, caused by the d^3 electron configuration sintering of Mn^{IV} containing compounds is known to be kinetically extremely inhibited.[7] Hence, reproducible preparation of $Sr_7Mn_4O_{15}$ ceramics was observed to be difficult and therefore less suitable for industrial production.

Oxide ceramic semiconductors based on the perovskite type structure are expected to be more available. Different from compounds of the spinel type, cation interchange between the dodecahedral A sites and the octahedrally coordinated smaller cations on B sites is energetically unfavourable and therefore unlikely. Disadvantageous for thermistor applications is the improved interaction of electron wave functions caused by corner-sharing of the octahedral units with bond angles near to 180° at the linking oxygens forming a three-dimensionally interconnected network of $[BO_{6/2}]$ octahedra, which is typical for compounds crystallizing in the perovskite type structure. Hence, relatively high conductivity values and low activation energies or even metallic behaviour are often found for perovskites containing transition metal ions of unsaturated d electron configuration or mixed oxidation states at the B sites. Commonly, the thermistor sensitivity for temperature measurement is entirely insufficient.

$BaTiO_3$ is n-type conducting after treatment in a reducing atmosphere at high temperature due to oxygen defect formation corresponding to $BaTi_{1-2x}^{IV}Ti_{2x}^{III}O_{3-x}V_{O,x}$. For $x=0.002$ the value $\sigma_{25°C}=5.6\ \Omega^{-1}cm^{-1}$ with an activation energy of 0.06 eV or $B=700$ K has been reported.[8] PTC ceramis based on donor doping, e.g. by substitution of a rare earth metal M^{III} for Ba^{II} in the series $Ba_{1-x}M_x^{III}Ti_{1-x}^{IV}Ti_x^{III}O_3$ provide even a lower value, e.g. $\sigma_{25}=2\ \Omega^{-1}cm^{-1}$.[9,10] Single crystals of $SrTiO_3$, whose oxygen defect concentration is formed by oxygen loss at high temperature corresponding to $SrTi_{1-2x}^{IV}Ti_{2x}^{III}O_{3-x}V_{O,x}$ achieve already at $x=0.00025$ a room temperature conductivity of 10 Ω^{-1} cm^{-1} showing a temperature coefficient which strongly indicates metallic behaviour.[11] $LaCoO_3$ has a room temperature conductivity of about 100 $\Omega^{-1}cm^{-1}$ with metallic behaviour above 330°C.[12,13] $La_{0.7}Sr_{0,3}CoO_3$ shows a conductivity value even of 1500 $\Omega^{-1}cm^{-1}$ at room temperature decreasing with temperature.[14]

Starting from $LaCoO_3$, it is the purpose of this paper to achieve increasing values of the activation energy by suitable substitution. Replacing pairs of Ti^{IV} and Co^{II} for $2Co^{III}$ corresponding to $LaTi_y^{IV}Co_y^{II}Co_{1-2y}^{III}O_3$ suggests an appropriate way in order to reduce the interaction of wave functions thus leading to localized polaron states. The activation energy of charge carriers will increase because of the random distribution of the differently charged cations at the B sites of the lattice. Of course, thermal excitation of the d electrons forming localized polaron states at the transition metal ions must increase with increasing fluctuations of the potential energy at the lattice sites, which implies increasing values of the activation energy of conduction. Within the limits $0.2<x<0.5$, studies have already been published.[15]

Partial substitutions of Sr for La corresponding to $Sr_xLa_{1-x}Ti_{x+y}^{IV}Co_y^{II}Co_{1-x-2y}^{III}O_3$ as an additional variati n is expected to extend the possibilities for selecting suitable compositions with desired values of the electrical properties. Therefore, variations of the ratio of Sr/La and Ti/Co are carried out in the limits $0<x<1$ and $0<y<(1-x)/2$. Published data[16] based on the coupled substitution of Sr for La and Ti for Co in the series $Sr_{1-x}La_xTi_{1-x}Co_xO_3$ will be compared with the results.

2. Ceramic sample preparation and X-ray diffraction measurements.

The formation of single phase perovskite ceramics in the series $Sr_xLa_{1-x}Ti_{x+y}^{IV}Co_y^{II}Co_{1-x-2y}^{III}O_3$ requires high temperatures and highly reactive powders. They have to be ground to an average size <1 μm. Hence, there is a danger for contamination of foreign impurities.

Following the mixed oxide route, the preparation starts from mixtures of the reagent grade raw materials

La_2O_3, $SrCO_3$, TiO_2 and Co-oxide, whose metal contents had been accurately determined by analysis. The weighing-out loss of the mixture of the components was ball milled in an aqueous slurry for 24 h using agate spheres. After evaporation of the water, drying and sieving, the powder mixture was heated up to 1250°C for 6 h for calcination using a ceramic setter material which had been saturated at the surface by pre-reaction with Co-oxide or with the synthesized powder itself. Repeating of this treatment is required in order for the reaction of perovskite type phase formation to proceed. Final phase formation succeeds only at sintering conditions. Therefore, the powder obtained from calcination was subjected to grinding again using an aqueous slurry and 1 mm spheres of Y_2O_3 stabilized zirconia in a shearing mill. An average grain size of 1–2 μm is easily achieved. After drying and sieving, the powder was again heated at 1250°C for 6 h. After this second step of calcination, final grinding of the powder was carried out with the use of 1 cm spheres of Y_2O_3 stabilized zirconia yielding an average grain size of about 0.8 μm followed by 1 mm spheres thus making it possible to achieve an average grain size of about 0.5 μm in a shorter time. Stepwise grinding leads to reduced contamination of ZrO_2. Despite careful handling, abrasive contamination of about 0.2% ZrO_2 was still observed due to powder processing.

After granulation using a polyvinyl alcohol binder, cylindrical discs have been formed by pressing. The opposite sides of the green bodies were coated for metallization using a Pt paste without glass frit. Heating up to about 450°C in air using a low heating rate of 0.6 K per minute for de-binding is immediately followed by a rate of 6 K per min up to 1350°C and keeping this temperature 1 h for sintering. In order to minimize losses of CoO by evaporation, a loosely closed alumina vessel was found to be suitable. Its surface was saturated with cobalt oxide by pre-reaction. Due to the basicity of the constituent oxides SrO and La_2O_3, oxygen loss from the bound cobalt(III) oxide does not occur even at the comparatively high sintering temperature. Variation of the cooling rate or keeping at a lower temperature, e.g. at 1000°C for 2 h, after sintering provide samples, whose electrical properties did not significantly show a difference to those prepared by rapid cooling. Commonly, a cooling rate of 6 K per min has been used after sintering.

Sintering aids, e.g. additions of 1 wt.% Bi_2O_3 do not make possible sintering at lower temperature. Perovkite type phase formation was observed to remain incomplete at lower temperatures, e.g. at 1300°C and also as a result of prolongated heating at this temperature. Due to residual heterogeneity in the ceramic structure, aging of the electrical data was always found to occur.

Simultaneously, together with the Pt contacted green bodies, samples without Pt electrodes were sintered for measuring the density and also for X-ray diffraction studies. Moreover, electrical contacts using a Ag paste without glass frit were burnt by firing at 800°C in order to compare the electrical properties with those obtained as a result of cofiring with Pt.

X-ray diffraction measurements were carried out using CuK_α radiation. The interpretation applying the LAZY PULVERIX programme and Rietveld refinement reveals that trigonal and orthorhombic distortion and also the cubic perovskite type structure occur as a function of the parameters x and y in the series $Sr_xLa_{1-x}Ti^{IV}_{x+y}Co^{II}_yCo^{III}_{1-x-2y}O_3$. The theoretical density ρ_{th} deduced from $\rho_{th} = z*M/V_{ec}*N_A$ with M as the mol weight of the formula unit, z as the number of units in the elementary cell with volume V_{ec} and N_A as the Avogadro number make it possible to calculate the relative density ρ_{rel} from the measured values ρ_{exp}.

The composition of the ceramic samples, their density values and crystallographic data are given in Table 1.

$LaCoO_3$ has a rhombohedral structure with $a_{rh} = 538.0$ pm, $\alpha = 60.81$ and $z = 2$ in the elementary cell, i. e. the rhombohedra are upset distorted along the [111] direction ($\alpha > 60°$). Data from the literature for $LaCoO_3$ are $a_{rh} = 537.8$ pm and $\alpha = 60.75°$ indicating that the trigonal distortion is increasing with temperature.[12,13] Table 1 shows the lattice parameter resulting from hexagonal interpretation. Corresponding to $a_{hex} = 2*a_{rh}*\sin(\alpha/2)$ and $c_{hex} = 3*a_{hex*}$ $\{1/[4\sin^2(\alpha/2)] - 1/3\}^{1/2}$ they are related to the rhombohedral one. Cubic symmetry ($\alpha = 60°$) provides the ratio $c_{hex}/a_{hex} = 2.4495$. With increasing substitution of pairs of Ti^{IV}/Co^{II} for 2 Co^{III} and pairs of Sr^{II} /Ti^{IV} for La^{III}/Co^{III} in the series the upset trigonal distortion is observed to be lowered. A change to orthorhombic distortion is found in the scope of lower Sr^{II} content ($x < 0.2$) when the y values approach the upper limit of substitution. On the other hand, in the range of higher content of Sr^{II} and Ti^{IV} the data of the ratio c_{hex}/a_{hex} indicate a change from trigonal upset distortion to stretching. At the same time the mole volume per formula unit $V_M = V_{hex*}N_A/6$ deduced from $V_{hex} = (3)^{1/2}a^2_{hex}c_{hex}/2$ for the hexagonal samples is increasing from 33.77 to 35.95 cm^3/mol. The highest values of 36.6 or 36.3 cm^3/mol are found for the orthorhombic distorted and cubic samples.

3. Electrical resistivity measurements and aging

For all of the batches, at least 24 cylindrical specimens with a diameter of about 3.0 mm and a height of 1.5 mm, prepared by co-firing with Pt electrodes, were measured. Measuring at 25 and 100°C provides the average value of the specific electrical resistivity $\rho_{25°C}$ and the value of $B_{25/100°C}$ deduced from the Arrhenius equation $\rho = \rho_N \exp[B/T]$. The data are given in Table 2.

Table 1
Density and data from X-ray diffraction measurements of selected compositions of the series $Sr_xLa_{1-x}Ti^{IV}_{x+y}\ Co^{II}_yCo^{III}_{1-x-2y}O_3$

Sample number	x	y	$\rho_{exp.}$/g cm^{-3}	ρ_{rel}/%	Lattice parameter (pm)	c_{hex}/a_{hex}	V_M (cm^3/mol)	Structure
0/1	0	0	6.87	94.4	$a_{hex}=544.62$ $c_{hex}=1309.71$	2.4048−1.82%	33.77	Rhombohedral $z_{rh}=2$, $z_{hex}=6$
0/5	0	0.20	6.87	94.4	$a_{hex}=548.74$ $c_{hex}=1321.45$	2.4082−1,69%	34.59	Rhombohedral $z_{rh}=2$, $z_{hex}=6$
0/6	0	0.4	6.38	96.0	$a_{orh}=555.23$ $b_{orh}=783.72$ $c_{hex}=554.64$		36.34	Orthorhombic $z=4$
0/8	0	0,45	6.25	95.0	$a_{orh}=556.98$ $b_{orh}=785.54$ $c_{hex}=555.56$		36.60	Orthorhombic $z=4$
1/1	0.1	0.10	6.87	98.9	$a_{hex}=546.86$ $c_{hex}=1321.12$	2.4158−1.37%	34.35	Rhombohedral $z_{rh}=2$, $z_{hex}=6$
1/3	0.1	0.30	6.41	96.3	$a_{orh}=550.13$ $b_{orh}=778.65$ $c_{hex}=553.03$		35.67	Orthorhombic $z=4$
2/1	0.2	0.05	6.50	96.1	$a_{hex}=546.72$ $c_{hex}=1324.74$	2.423−1.08%	34.42	Rhombohedral $z_{rh}=2$, $z_{hex}=6$
2/6	0.2	0.15	6.54	98.5	$a_{hex}=549.23$ $c_{hex}=1330.50$	2.4225−1.10%	34.89	Rhombohedral $z_{rh}=2$, $z_{hex}=6$
2/9	0.2	0.30	6.19	97.0	$a_{orh}=552.34$ $b_{orh}=781.47$ $c_{hex}=554.66$		36.05	Orthorhombic $z=4$
3/1	0.3	0	6.44	97.7	$a_{hex}=546.46$ $c_{hex}=1327.73$	2.430−0.80%	34.47	Rhombohedral $z_{rh}=2$, $z_{hex}=6$
3/2	0.3	0,05	6.21	95.6	$a_{hex}=548.65$ $c_{hex}=1332.72$	2.429−0.90%	34.88	Rhombohedral $z_{rh}=2$, $z_{hex}=6$
3/5	0.3	0,18	6.15	96.65	$a_{hex}=551.43$ $c_{hex}=1338.59$	2.4275−0.90%	35.385	Rhombohedral $z_{rh}=2$, $z_{hex}=6$
3/7	0.3	0,22	6.11	96.7	$a_{hex}=550.21$ $c_{hex}=1351.32$	2.456+0.265%	35.56	Rhombohedral $z_{rh}=2$, $z_{hex}=6$
4/1	0.4	0	6.10	95.3	$a_{hex}=544.94$ $c_{hex}=1337.41$	2.454+0.18%	34.53	Rhombohedral $z_{rh}=2$, $z_{hex}=6$
4/2	0.4	0.04	6.05	95.0	$a_{hex}=545.02$ $c_{hex}=1340.38$	2.459+0.40%	34.61	Rhombohedral $z_{rh}=2$, $z_{hex}=6$
4/6	0.4	0.1	5.91	93.9	$a_{hex}=546.12$ $c_{hex}=1346.66$	2.466+0.67%	34.92	Rhombohedral $z_{rh}=2$, $z_{hex}=6$
4/9	0.4	0.135	6.07	97.8	$a_{hex}=550.98$ $c_{hex}=1340.48$	2.433-0.68%	35.38	Rhombohedral $z_{rh}=2$, $z_{hex}=6$
4/11	0.4	0.2	5.89	96.4	$a_{hex}=553.07$ $c_{hex}=1346.71$	2.435−0.59%	35.78	Rhombohedral $z_{rh}=2$, $z_{hex}=6$
5/1	0.5	0	5.88	94.9	$a_{hex}=545.43$ $c_{hex}=1339.79$	2.456+0.28%	34.65	Rhombohedral $z_{rh}=2$, $z_{hex}=6$
5/3	0.5	0.08	5.65	92.7	$a_{hex}=548.81$ $c_{hex}=1339.01$	2.440−0.39%	35.06	Rhombohedral $z_{rh}=2$, $z_{hex}=6$
5/7	0.5	0.2	5.67	97.0	$a_{cub}(1)=391.41$ $a_{cub}(2)=393.03$		36.3	Cubic $z=1$
6/2	0.6	0.018	5.60	94.5	$a_{hex}=548.99$ $c_{hex}=1341.65$	2.444−0.23%	35.15	Rhombohedral $z_{rh}=2$, $z_{hex}=6$
6/10	0.6	0.14	5.43	94.4	$a_{hex}=553.45$ $c_{hex}=1349.98$	2.440−0.42%	35.95	Rhombohedral $z_{rh}=2$, $z_{hex}=6$
7/2	0.7	0.02	5.40	94.7	$a_{hex}=549.78$ $c_{hex}=1348.81$	2.453+0.16%	35.44	Rhombohedral $z_{rh}=2$, $z_{hex}=6$

In accordance with expectation, starting from $LaCoO_3$ with $\rho_{25°C} = 1.9$ Ωcm and the comparatively low value of $B = 1765$ K, changing the values of x and y in the substitutional series $Sr_xLa_{1-x}Ti^{IV}_{x+y}\ Co^{II}_yCo^{III}_{1-x-2y}O_3$ makes possible to vary the electrical properties in a wide range. For a given level of x the values $\rho_{25°C}$ and $B_{25°C/100°C}$ increase with y, i.e. when Ti^{IV}/Co^{II} pairs are substituted for 2 Co^{III}. In the range $x \leqslant 0.3$, values $B_{25°C/100°C}$ up to about 3000 K coupled with $\rho_{25°C} \leqslant 20$ Ωcm may be achieved, which is of interest for insurance NTC applications.[17] On the other hand, NTC ceramics with values $B_{25°C/100°C}$ up to about 6500 K can be prepared yielding sufficient sensitivity values even at higher temperature. Hence, in close relation with the thermal stability of the structure of the perovskite type ceramics high temperature thermistor applications have been proposed.[17,18]

Figs. 1 and 2 show the variation of the electrical data $1/\rho_{25°C}$ and $B_{25°C/100°C}$ as a function of x and y in the series $Sr_xLa_{1-x}Ti^{IV}_{x+y}\ Co^{II}_yCo^{III}_{1-x-2y}O_3$. Interpolation suggests to choose a composition providing pre-determined electrical data of NTC ceramics. For aging a set of four samples was subjected to annealing using the temperatures 80, 100, 150, 200 300 and 500°C. After soaking for 72 h, the samples were removed from the thermostat for cooling in air. Measuring of the electrical resistivity at 25 and 100°C was carried out and annealing was proceeded at the same temperatures up to 144 h or more followed by measuring again. The differences between these values and the initial data

Table 2
Specific resistivity $\rho_{25°C}$ and the values $B_{25/100°C}$ of ceramic samples in the series $Sr_xLa_{1-x}Ti^{IV}_{x+x}Co^{II}_yCo^{III}_{1-x-2y}O_3$ co-fired with Pt electrodes: sample diameter 3 mm, thickness 1.5 mm[a]

Sample number	x	y	$\frac{\rho_{25C}}{\Omega cm}$	$B_{25\%100°C}$ (K)	Sample number	x	y	$\frac{\rho_{25C}}{\Omega cm}$	$B_{25\%100°C}$ (K)
0/1	0	0	1.92±4%	1765±1.3%	4/4	0.4	0.062	85.2±4%	2819±0.3%
0/2	0	0.1	1.11±2%	1913±2.1%	4/5	0.4	0.08	105.4±5%	2953±0.5%
0/3	0	0.13	2.59±3%	2212±1.4%	4/6	0.4	0.10	202.±4%	3181±0.5%
0/4	0	0.17	9.25±2.4%	2692±0.3%	4/7	0.4	0.12	794±4%	3778±0.5%
0/5	0	0.18	16.8±3%	2970±0.3%	4/8	0.4	0.126	1283±5%	3922±0.5%
0/6	0	0.20	44.8±5%	3370±0.2%	4/9	0.4	0.135	2411±5%	4162±0.6%
0/7	0	0.30	9028±5%	5351±0.1%	4/10	0.4	0.18	65 700±5%	5061±0.4%
0/8	0	0.40	65 9940±4%	6085±0.06%	4/11	0.4	0.20	205 500±5%	5448±0.6%
0/9	0	0.45	8.09×10^6±15%	6875±0.8%	4/12	0.4	0.24	3×10^6±4%	5888±0.2%
1/1	0.1	0.10	3.77±4%	2268±0.5%	4/13	0.4	0.28	51.7×10^6±4%	6365±0.4%
1/2	0.1	0.20	221.±3%	3839±0.3%	5/1	0.5	0	216±4%	3119±0.2%
1/3	0.1	0.30	33 620±3%	5555±0.1%	5/2	0.5	0.04	220±5%	2962±0.5%
1/4	0.1	0.40	8.1 10^6±3%	6548±0.2%	5/3	0.5	0.08	702±5%	3314±0.2%
2/1	0.2	0	6.66±3%	2505±0.5%	5/4	0.5	0.0975	3676±5%	3936±0.5%
2/2	0.2	0.05	6.04±3%	2319±0.3%	5/5	0.5	0.105	5656±5%	4199±0.5%
2/3	0.2	0.10	13.62±3%	2549±0.3%	5/6	0.5	0.135	42 668±3%	5176±0.2%
2/4	0.2	0.124	30.96±4%	2875±0,5%	5/7	0.5	0.20	11.7×10^6±5%	6103±0.06%
2/5	0.2	0.1256	33.7±5%	2873±0.5%	6/1	0.6	0	1126±5%	3299±0.4%
2/6	0.2	0.13	36.5±2%	2930±0.3%	6/2	0.6	0.018	1097±3%	3260±0.1%
2/7	0.2	0.15	93.46±3%	3314±0.3%	6/3	0.6	0.020	1223±3%	3274±0.1%
2/8(Pt)	0.2	0.176	469±1.5%	3869±0.08%	6/4	0.6	0.040	1350±5%	3378±0.4%
2/8(Ag)	0.2	0.176	444±1.5%	3863±0.07%	6/5	0.6	0.050	2593±5%	3541±0.6%
2/9	0.2	0.20	1539±3%	4422±0.2%	6/6	0.6	0.0556	4203±4%	3709±0.4%
2/10	0.2	0.25	25 825±5%	5294±0.1%	6/7	0.6	0.058	5091±3%	3816±0.4%
2/10	0.2	0.30	253 540±4%	5783±0.1%	6/8	0.6	0.062	6065±5%	3877±0.6%
2/11	0.2	0.35	5.01 10^6±3%	6279±0.07%	6/9	0.6	0.065	7598±5%	3986±0.6%
3/1	0.3	0	18.67±4%	2683±0.6%	6/10	0.6	0.10	76 630±5%	4796±0.5%
3/2	0.3	0.05	19.74±2.5%	2458±0.4%	6/11	0.6	0.14	1.30×10^6±5%	5810±0.2%
3/3	0.3	0.10	55.05±3%	2897±0.6%	6/12	0.6	0.15	6.5×10^6±5%	6144±0.3%
3/4	0.3	0.14	317.1±3%	3584±0.3%	6/13	0.6	0.16	15.5×10^6±5%	6251±0.4%
3/5	0.3	0.18	4282±4%	4626±0.4%	7/1	0.7	0	7804±4%	3534±0.4%
3/6	0.3	0.20	19 871±4%	5152±0.2%	7/2	0.7	0.02	11 590±4%	3676±0.3%
3/7	0.3	0.22	54 26±4%	5537±0.2%	7/3	0.7	0.04	30 950±2%	4024±0.6%
3/8	0.3	0.28	952 000±4%	5893±0.1%	7/4	0.7	0.06	127 300±5%	4630±0.6%
4/1	0.4	0	58.83±4%	2804±0.5%	7/5	0.7	0.08	556 220±5%	5183±0.8%
4/2	0.4	0.02	57.0±3%	2727±0.6%	8/1	0.8	0	62 615±5%	3682±0.5%
4/3	0.4	0.04	60.0±2%	2708±0.2%					

[a] Sample diameter 3mm, thickness 1.5mm

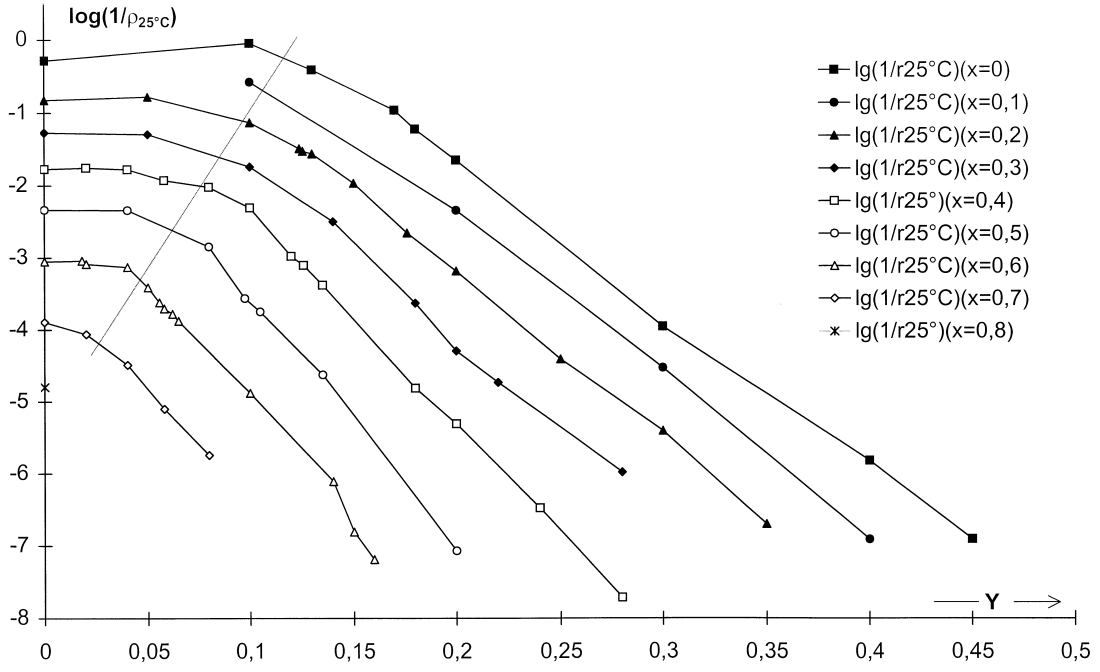

Fig. 1. Specific conductivity $\log(1/\rho_{25^\circ C})$ as a function of y in the series $Sr_xLa_{1-x}Ti^{IV}_{x+y}Co^{II}_yCo^{III}_{1-x-2y}O_3$.

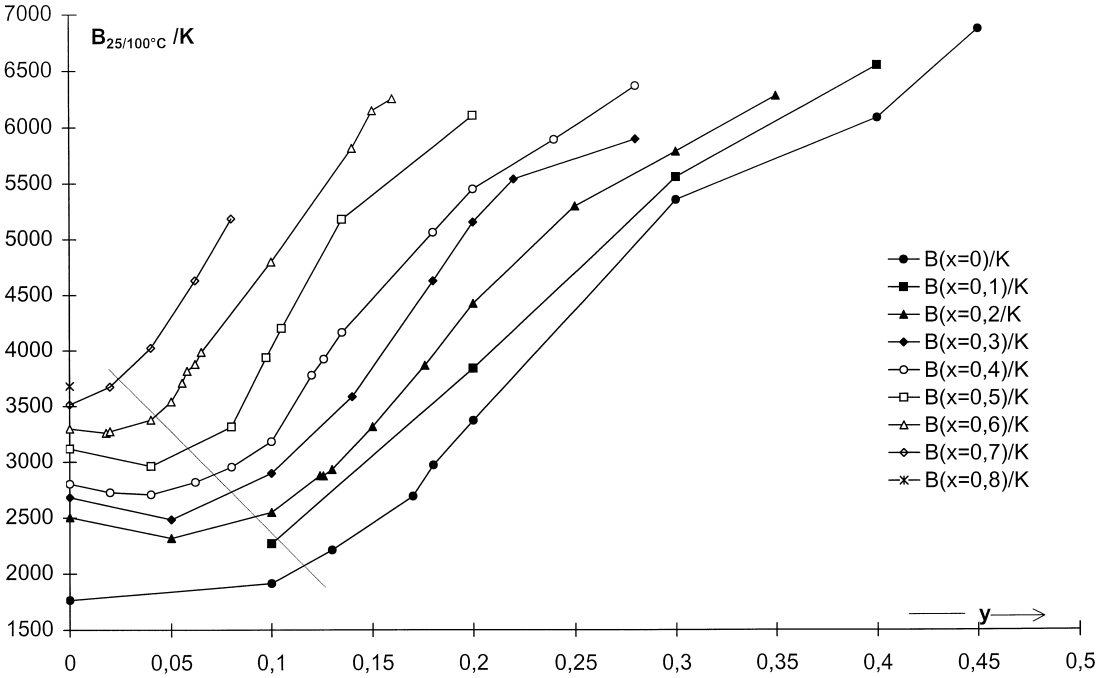

Fig. 2. Values $B_{25/100^\circ C}$ as a function of y in the series $Sr_xLa_{1-x}Ti^{IV}_{x+y}Co^{II}_yCo^{III}_{1-x-2}O_3$.

lead to the values of $\Delta\rho_{25^\circ C}/\rho_{25^\circ C}$ which indicate vanishing aging, provided single phase state formation of the perovskite type structure could completely be achieved as a result of ceramic preparation and sintering. However, it has to be noted that the single phase state is the more hardly achieved the higher the x values, e.g. $x=0.7$ or 0.8. For $x<0.7$, in the range of the lowest and at the highest values of y approximate zero aging is also missing. In this scope aging values of $\Delta\rho_{25^\circ C}/\rho_{25^\circ C}=$ 0.1–1% or more may occur. Typical residual variations of $\Delta\rho_{25^\circ C}/\rho_{25^\circ C}$ in the range of homogeneous perovskite type formation are observed to be restricted

to ±0.01–0.1% during heating at 500°C for several hundred hours.

As an example, for the composition of $Sr_{0.2}La_{0.8}Ti^{IV}_{0.376}Co^{II}_{0.176}Co^{III}_{0.448}O_3$ the electrical properties of specimens with co-fired Pt electrodes are compared with those, whose Ag contacts were separately fired after sintering. Good agreement is observed as can be seen from the data of sample 2/8(Pt) and 2/8(Ag) of Table 2. The result infers the assumption that the properties of the bulk ceramics prevail. Therefore, the omission of contact barriers at the electrodes is justified to be a sufficient approximation. Seebeck effect measurements of $LaCoO_3$[19] and of samples in the series $Sr_{1-x}La_xTi_{1-x}Co_xO_3$ with $0.1 < x < 0.4$[16] provide a positive sign of charge carriers. Hence, even for nobel metals the formation of an enrichment zone at the ceramic electrode boundary seems to be favoured.

It has to be noted that the conductivity values $\rho_{25°C}$ of the samples 6/1, 7/1, and 8/1 of Table 2 are by several orders of magnitude lower and the *B*-values significantly smaller than the published data.[16] On the other hand, the values of the samples 0/6, 0/7 and 0/8 are consistent with the data which have already been reported in the literature.[15]

4. Discussion

Figs. 1 and 2 suggest to assume a change of the mechanism of charge carrier transport in the series $Sr_xLa_{1-x}Ti^{IV}_{x+y}Co^{II}_yCo^{III}_{1-x-2y}O_3$ when the values of x and/or y are increasing. In an area labelled by the dotted line, i.e. for small values of y, the specific conductivity $\sigma_{25°C} = 1/\rho_{25°C}$ and the values of $B_{25°C/100°C}$ show comparatively small changes as a function of composition. This scope is found to be the more extended with y the smaller the x values. Such a behaviour is found to be related to high concentrations of Co^{III} in the trigonally distorted perovskite type lattice deduced from $LaCoO_3$. On the other hand, at the right hand side of the dotted line, extended substitution of Ti^{IV} and/or Co^{II} for Co^{III} leads in close relation with the variation of x and y to decreasing values of the conductivity and increasing values of the B constant. At high values of y, the electrical data reflect the change from the trigonal distorted to the orthorhombic structure in correspondence with the crystallographic data of Table 1.

Polaron state formation has been widely accepted as a suitable concept for interpretation of charge carrier transport phenomena of semiconductors based on transition metal oxides. If N_t is the total number of sites in volume V that can be occupied by a charge carrier in combination with thermally activated hopping and ω is the probability of their occupation, the charge carrier density is given by $n = N_t\omega/V$. With the probability $(1-\omega)$ for the existence of vacant positions at the jump distance a and jump probability ν (hopping frequency), the diffusion coefficient is given by the expression

$$D = a^2(1-\omega)\nu$$

$$= a^2(1-\omega)\nu_0 \exp(-E_A/kT)\exp(-2\gamma a) \quad (1)$$

ν_0 is an average phonon frequency and $\exp(-2\gamma a)$ is an overlap factor which represents the attenuation of the wave function of the electron or defect electron over the jump distance a. The diffusion coefficient and the mobility are connected by the Nernst–Einstein relation $\mu = eD/kT$, which, together with $\sigma = ne\mu$ leads to the conventional expression for hopping conduction

$$\sigma = \frac{ne^2D}{kT} = \frac{n(1-\omega)e^2a^2\nu_0}{kT}\exp(-E_A/kT)$$
$$\exp(-2\gamma a) = ne\mu_0 \exp(-E_A/kT) \quad (2)$$

with $E_A = B/k$ as the activation energy. Finally, the carrier density n can be replaced by the expression $n = N_t\omega/V$ with N_t as the total number of Co ions in the volume V of the sample. If the ratio $N_t/V = n_t/a^3$ with n_t as the number of Co ions in the jump volume a^3 is used, Eq. (2) then leads to

$$\sigma = (1/\rho_{25°C})$$

$$= \frac{n_1\nu_0e^2}{akT}\omega(1-\omega)\exp(-B/T)\exp(-2\gamma a) \quad (3)$$

At a given temperature, the conductivity is a function of the average distance a of the lattice positions which may be occupied by charge carriers with the probability ω or they are empty according to $(1-\omega)$. The probability ω for the occupied B sites corresponds to the mole fraction x_{CoII} and the probability $(1-\omega)$ can be interpreted as the mol fraction x_{CoIII} of vacant sites. Ti^{IV} should not take part in the mechanism of charge carrier transport because Ti^{III} should be unstable in the presence of Co^{III}. Ti^{IV}/Co^{II} pairs are energetically preferred. Moreover, the conductivity is assumed to depend strongly on the internal barrier profile thus formed by fluctuations of the potential energy as a result of random distribution of the cations of different charge at the A and B sites of the perovskite type structure of $Sr_xLa_{1-x}Ti^{IV}_{x+y}Co^{II}_yCo^{III}_{1-x-2y}O_3$.

At low temperature the low spin-state t_{2g}^6 of the Co^{III} ions of $LaCoO_3$ is assumed to be more stable than the high spin state.[20] Measurements of the electrical and magnetic properties as a function of temperature elucidate substantial population of an intermediate state $t_{2g}^5e_g^1(\sigma^*)^1$[12] and the presence of the high spin configuration $t_{2g}^4e_g^2$ (σ^*) has also been taken into consideration.[12,13] The energies of the intermediate state and of the high spin state measured from the low spin state were

estimated to be 0.02 and 0.1 eV, respectively. The t_{2g} electron states are favoured to form polaron band states in the gap because of suitable dπpπ interaction between the transition metal ions at the B sites and the oxygen ions in the perovskite type structure. As a consequence of trigonal lattice distortion, sub-band formation resulting from splitting of the t_{2g} states into e_g and a_1 states has to be taken into account. This is shown in Fig. 3(a). For an upset distorted octahedral network small e_g polaron band states are expected to form the highest occupied states. However, due to the low values of the excitation energy an essential part of the Co^{III} ions is in the intermediate or even in the high spin state thus leading to localized polaron states. Electrons at the anti-bonding $e_g(\sigma^*)$ states are expected to be more localized because of the less suitable symmetry adaption of the interacting wave functions. Of course, as shown by the scheme of Fig. 3(b), in comparison with the negatively charged $e_g^1(\sigma^*)$ polaron states defect polaron hopping events of e_g^3 states should be preferred due to the suitable interaction with adjacent occupied states. Following the intentions of Mott,[21] the adiabatic approximation of polaron hopping with $\exp(-2\gamma a)\approx 1$ is suggested to be valid. d–d transitions are always coupled with lattice vibrations and many hopping events are enabled to occur during the life time of the excited intermediate or high spin state. The trigonal upset distortion has been shown to increase with temperature and at the same time due to improved interaction of the wave functions the value of the Seebeck coefficient having a positive sign is also increasing.[13]

Therefore, corresponding to $\sigma = ne\mu_e + pe\mu_p$ the contribution of defect electron charge carrier transport to the entire conductivity prevails. Fig. 3(c) shows schematically that this situation can be widely maintained at low y values in the series because there are only some more $e_g^1(\sigma^*)$ states labelling together with the attributed a_{1g}^2/e_g^4 occupation the positions of Co^{II} ions at the B sites. However, corresponding to the formula $Sr_xLa_{1-x}Ti^{IV}_{x+y}Co^{II}_yCo^{III}_{1-x-2y}O_3$, increasing substitution of pairs of Ti^{IV}/Co^{II} for 2 Co^{III} caused by the increasing values of y implies dilution of the interacting Co^{III} ions, i. e. polaron band formation becomes more and more interrupted and the average value of the hopping distance a is increasing. At the same time increasing random fluctuations of the potential energy at the B sites generates also more localization with increasing values of y. These effects will be strengthened when the parameter x is also different from zero, i.e. if pairs of Sr^{II}/Ti^{IV} for La^{III}/Co^{III} are additionally introduced into the lattice. Consequently, as shown in Fig. 3(d) the activation energies of hopping between strongly localized Co^{III} polaron states $e_g^3/e_g^1(\sigma^*)$ and Co^{II} polaron states $e_g^4/e_g^1(\sigma^*)$ will predominate in the mechanism of charge carrier transport the more the higher the values of x and y. In this scope of extended localization the so-called non-adiabatic approximation has to be taken into consideration because there is a probability $\exp(-2\gamma a) < 1$ of the electron transfer during the period of a lattice vibration.

The curves of the series shown in Figs. 1 and 2 imply variations of the mole fractions x_{CoII} and x_{CoIII} and at the same time the total concentration of Co is changing, i.e. the average distance a between the d electron bond centers which are involved into hopping transport is altered. Due to increasing random fluctuation of the potential energy between the lattice positions the activation energy of hopping transport covers a wide range of values with increasing values of x and y.

Fig. 4 shows a plot of the B values and of the specific conductivity as a function of the Co^{III} concentration for

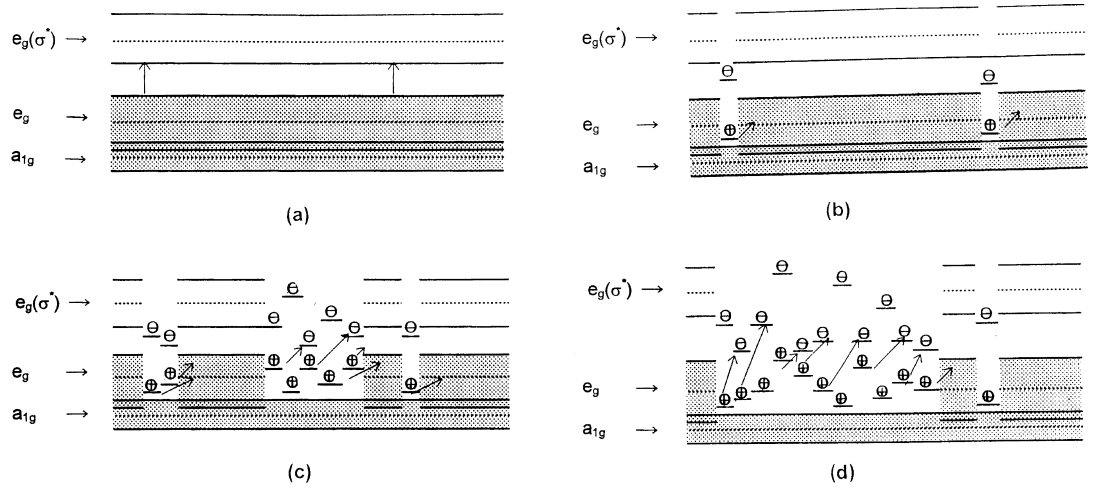

Fig. 3. Scheme of t_{2g} band states at trigonal distortion (a), formation of localized polaron states as a result of d–d electron transitions from the low spin to an intermediate high spin state opening the possibility of hopping without disproportionation of Co^{III} (b), and transfer to hopping of charge carriers between Co^{II} and Co^{III} polaron states in the result of increasing localization caused by random substitution in the series $Sr_xLa_{1-x}Ti^{IV}_{x+y}Co^{II}_yCo^{III}_{1-x-2y}O_3$ when y is increasing (c) and x is increasing, too (d).

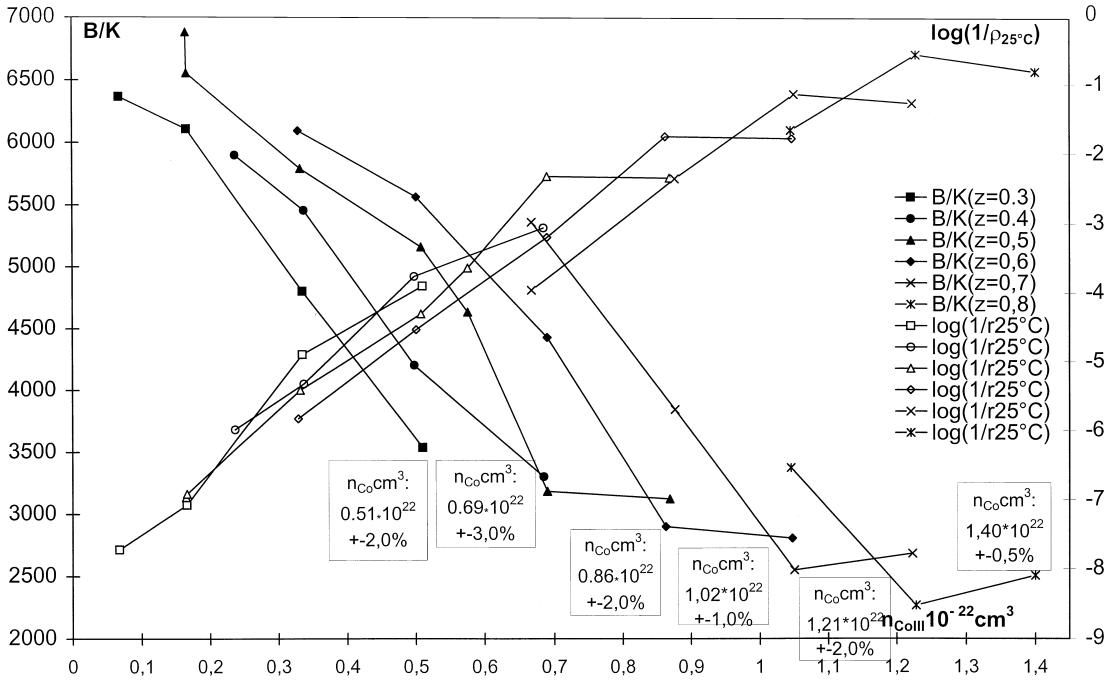

Fig. 4. Variations of the values of $B_{25/100°C}$ and $\log(1/\rho_{25°C})$ as a function of the concentration of Co^{III} in the lattice for series $Sr_xLa_{1-x}Ti^{IV}_{x+y}$ $Co^{II}_yCo^{III}_{1-x-2y}O_3$ with the total concentration $z=1-(x+y)=$constant.

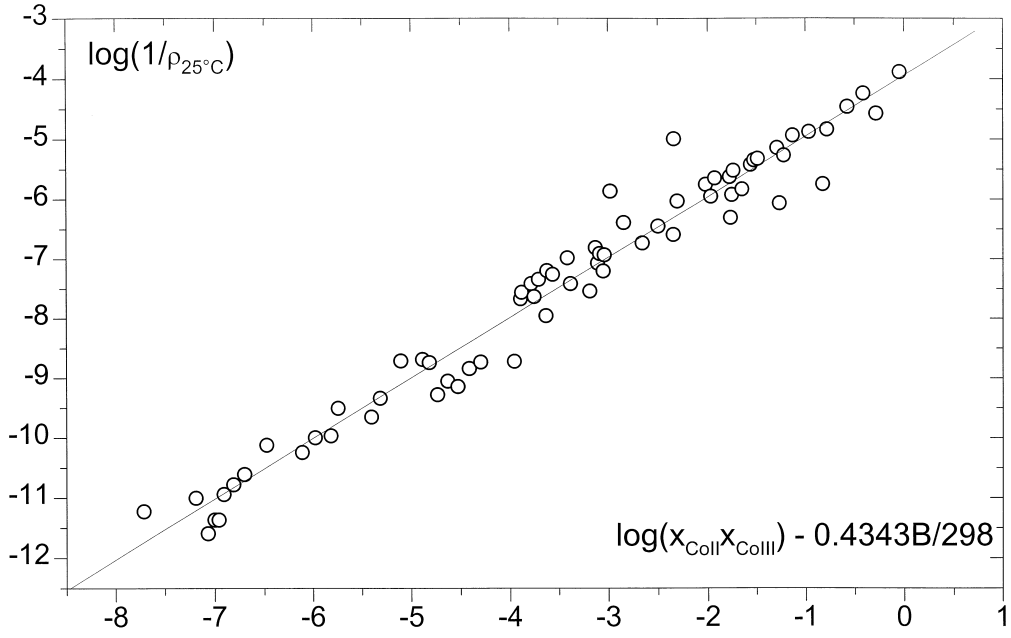

Fig. 5. Plot of $\log(1/\rho_{25°C})$ versus $\log(x_{CoII}x_{CoIII})-0.4343B/298$ according to Eq. (4)..

constant values of the total concentration of Co. Corresponding to the formula $Sr_xLa_{1-x}Ti^{IV}_{x+y}Co^{II}_yCo^{III}_{1-x-2y}O_3$ the values of $z=1-x-y$ are constant, i. e. the Ti^{IV} concentration $(x+y)$ and also the average distance between the cobalt ions remain unchanged for the specimens attributed to one of the curves. Only the ratio of Co^{II}/Co^{III} is varying in these series. With increasing substitution of Sr^{II} for La^{III} according to x the content of y Co^{II} has to be reduced by the same value on behalf of the formation of Co^{III}. The values of n_{CoIII} are calculated using the data of the mole volume of Table 1. Series with an approximately constant average distance for polaron hopping suggest a strong correlation between $\log(1/\rho 25°C)$ and the values of the B constant.

At the highest Co^{III} concentrations the conductivity behaviour approaches $LaCoO_3$. On the other hand, deviations in the range of the lowest values of Co^{III} concentration correlate with the transition from trigonal to orthorhombic distortion. At the same time, the mol volume is increasing as shown by the values of Table 1. Using the equation

$$\log(1/\rho_{25^\circ C}) = \log\frac{n_1 v_0 e^2}{ak298} + \left[\log(x_{Co^{II}} x_{Co^{III}}) - 0.4343B/298)\right] \quad (4)$$

it seems to be possible to combine all of the electrical data. This is shown in the plot of Fig. 5. The slope of the straight line resulting from linear regression analysis is found to be near to 1, which is consistent with the proposed interpretation. Polaron hopping seems to be a suitable model for the analysis of the conductivity behaviour of this group of oxide ceramic semiconductors having a single phase perovskite type structure.

5. Conclusions

Ceramics based on perovskites of the series $Sr_xLa_{1-x}Ti^{IV}_{x+y}Co^{II}_yCo^{III}_{1-x-2y}O_3$ with $0<x<1$ and $0<y<(1-x)/2$ are found to be suitable for NTC semiconductor applications. The conductivity behavior can be interpreted by the conventional polaron state hopping model. The value of the specific resistivity $\rho_{25^\circ C}$ and the B - value are adjustable to desired values within the frame $\rho_{25^\circ C}=1.1$ Ωcm, $B=1910$ K and $\rho_{25^\circ C}=1$ to 8×10^6 Ωcm at B - values up to 6500 K. Therefore, dependent on the values of x and y, NTC thermistor and insurance applications have been proposed.[17,18] The thermistors do not show aging even at higher temperature, e.g. at 500°C, provided the single phase state is achieved as a result of mixed oxide preparation and sintering. Hence, high temperature thermistor applications are also made possible. The advantage of stability against aging at higher temperature is closely related to the defined structure of perovskite type compounds ABO_3, whose cations A and B are, independent of temperature, pinned at the lattice sites. On the other hand, because of the internal equilibria of cation redistribution, the spinel forming oxide systems which are usually applied as a thermistor material show aging when the temperature exceeds the limit of 150–200°C.

Acknowledgements

The author is indebted to Dr. Jörg Albering, Institute of Chemical Technology of Inorganic Materials of the Technical University Graz, for X-ray diffraction measurements and interpretation, and also Mrs. Margarethe Pölzl for careful preparation and Mrs. Monika Kogler for measuring the electrical data and aging of samples.

References

1. Feltz, A. and Pölzl, W., Spinel forming ceramics of the system $Fe_xNi_yMn_{3-x-y}O_4$ for high temperature NTC thermistor applications. *J. Eur. Ceram. Soc.*, 2000, **20**, 2353–2366.
2. Feltz, A., Sinterkeramik für NTC-Hochtemperatur-Thermistoren, Patent DE 99 P2730, 3. 9. 99.
3. Kriegel, R., Feltz, A., Walz, L., Simon, A. and Mattausch, H.-J., Über die Verbindung $Sr_7Mn_4O_{15}$ und Beziehungen zur Struktur von Sr_2MnO_4 und α-$SrMnO_3$. *Z. Anorg. Allg. Chem.*, 1992, **617**, 99.
4. Feltz, A., Kriegel, R. and Schrank, F., Sinterkeramik für stabile Hochtemperatur-Thermistoren und Verfahren zu ihrer Herstellung. EP 0638910 A1, US 5 536 449.
5. Feltz, A., Tendencies in the development and application of negative temperature coefficient oxide ceramics. *Proceed. Electroceramics IV, Aachen*, 1994, **II**, 677–684.
6. Feltz, A., Kriegel, R. and Pölzl, W., $Sr_7Mn_4O_{15}$ ceramics for high temperature NTC thermistors. *J. Mater. Sc. Lett.*, 1999, **18**, 1693.
7. Feltz, A., Jäger, M. and Völksch, G., Über den Mechanismus der Spinellbildung im System $Zn_xMn_{3-x}O_4$. *Z. Anorg. Allg. Chem.*, 1988, **562**, 73.
8. Gerthsen, P., Kauer, E. and Reik, H. G., Halbleitung einiger Übergangsmetalloxide im Polaronenbild. In *Festkörperprobleme Band* V. F. Sauter. (ed). Akademie-Verlag, Berlin, 1966.
9. Huybrechts, B., Ishizaki, K. and Takata, M., The positive temperature coefficient of resistivity in barium titanate. *J. Mater. Sci.*, 1995, **30**, 2463.
10. Sinclair, D.C and West, A. R., Use of succinic acid to test the stability of PTCR $BaTiO_3$ Ceramics under reducing conditions.. *J. Am. Ceram. Soc.*, 1995, **78**, 241.
11. Moos, R., Menesklou, W. and Härdtl, K.H, Hall mobility of undoped n-type conducting strontium titanate single crystals between 19 K and 1373 K. *Appl. Phys. A*, 1995, **61**, 389.
12. Thornton, G., Tofield, B. C. and Williams, D. E., Spin state equilibria and the semiconductor to metal transition of $LaCoO_3$. *Solid State Commun.*, 1982, **44**, 1213.
13. Asai, K., Yoneda, A., Yokokura, O., Tranquada, J. M., Shirane, G. and Kohn, K., Two spin-state transitions in $LaCoO_3$. *J. Phys. Soc. Jap*, 1998, **67**, 290.
14. Mineshige, A., Kobune, M., Fujii, S., Ogumi, Z., Inaba, M., Yao, T. and Kikuchi, K., Metal-insulator transition and crystal structure of $La_{1-x}Sr_xCoO_3$ and functions of Sr-content, temperature, and oxygen partial pressure. *J. Solid State Chem.*, 1999, **142**, 374.
15. Macher, A., Reichmann, K. O., Fruhwirth, O., Gatterer, K. and Herzog, G. W., Perovskite versus spinel type NTC materials for application at elevated temperatures. *Informacije MIDEM*, 1996, **26**, 79.
16. Parkash, O., Kumar, D. and Prasad, C. D., Electrical conduction in the $Sr_{1-x}La_xTi_{1-x}Co_xO_3$ ($x<0.4$) system. *J. Phys. D: Appl. Phys*, 1995, **27**, 1509.
17. Feltz, A., Sinterkeramik für hochstabile NTC-Einschaltstrombegrenzer und niederohmige NTC-Thermistoren, Patentschrift DE 198 34 423 C1.
18. Feltz, A., Sinterkeramik für hochstabile Thermistoren und Verfahren zu ihrer Herstellung, DE 197 40 262 C1.
19. Senaris, M. A. and Goodenough, J. B., Magnetic and transport properties of the system $La_{1-x}Sr_xCoO_{3-\delta}$ ($0<x<0.50$). *J. Solid State Chem.*, 1971, **5**, 323.
20. Senaris-Rodriguez, M. A. and Goodenough, J. B., $LaCoO_3$ revisited. *J. Solid State Chem.*, 1995, **116**, 224.
21. Mott, N. F. and Davis, E. A., *Electronic Processes in Non-crystalline Materials*, 2nd edn. Clarendon Press, Oxford, 1979.